Preprints of the 21st IFAC World Congress (Virtual)
Berlin, Germany, July 12-17, 2020

Wave propagation patterns in gas pipelines for fault location ⋆

Jesús Peralta * **Cristina Verde** * **Fermín Delgado** *

* *Instituto de Ingeniería, Universidad Nacional Autónoma de México (e-mail: JPeraltaC@iingen.unam.mx, verde@unam.mx, FDelgadoS@iingen.unam.mx).*

Abstract: Based on the reflectometry phenomenon and the behavior of an acoustic signal in a gas pipeline, this work proposes a fault location test for pipelines, which is formally justified for an infinite-dimension model of acoustic wave propagation in a closed conduit with viscous absorption. The test consists of disturbing the medium by an acoustic pulse at one extreme of the pipeline and of registering the transient response at an observation point. In this way, the waveform of the transient response of the pressure allows distinguishing the pattern of a healthy system from a pipeline with diverse faults and to allow locating the position of the damage.

Keywords: Feature selection for fault location, propagation model, waveform patterns.

1. INTRODUCTION

Faults in gas pipelines are a global problem (Verde and Torres, 2017). Several technologies have been proposed for detecting and locating fault scenarios. These include volume balance, pressure analysis, acoustic detection, thermographic analysis and radar signal processing (Datta and Sarkar, 2016).

The waves' reflection phenomenon produced by a leak in conduits has been used for more than 30 years for locating its position (Liu et al., 2017). Faults effects have been analyzed in the time domain by Brunone and Ferrante (2001) and in the frequency domain by Lee et al. (2005). It has also been shown that acoustic emissions are often much faster and much cheaper than other conventional hardware methods, such as tracer gas, infrared thermography, and ultrasonic and electromagnetic scanning (Ahadi and Sarif-Bakhtiar, 2010).

If pipeline installations are not instrumented, one option for locating faults is the use of off-line transient tests designed by considering the reflected waves caused by the fault. In this way, when an acoustic signal is injected into the medium, if a damage is present the acoustic impedance of the fluid changes (Meniconi et al., 2011). An advantage of these tests is that they require only an external perturbation signal and at some point of the duct a data register. This register collects the transient pressure for detecting abnormal events. This semi-automatic method requires an actuator for the injecting of the acoustic signal into the line and a pressure transducer that collects the signal and allows the identification of abnormal conditions in a short time with respect to the wave propagation speed c. This method is feasible if the wave propagation model in normal conditions is known. Moreover, this manoeuver can be used in transient events. Fig. 1 shows a possible configuration for this type of test. Thus, if a loudspeaker is located at position 0 upstream from a microphone located at position x_0 and a discontinuity or fault is present downstream from the microphone at x_1, the waveform of the pressure at the microphone is modified from its normal pattern. If the fluid behavior is assumed to be linear, the evolution of the pressure at the microphone can be approximated and analyzed from the fluid model. This means a specific perturbation is generated to determine the presence of faults. An advantage of this kind of maneuver is that the diagnosis can be achieved with exogenous acoustic signals that are generated as long as the fault is active.

This idea was developed by Vidal and Silva (2014) for designing a diagnosis device for gas pipelines. The formal propagation model of acoustic waves for different fault conditions, however, is missing in the work of Vidal. These facts motivate this work in which first the propagation model of acoustic waves with an attenuation caused by viscosity and faults is analytically derived by considering the partial differential equations (PDE) associated with the momentum and mass balance of a gas in a damaged pipeline. On the basis of the obtained model, the main contribution is developed. This consists of the characterization of the pressure's waveform and the respective line impedance for various types of faults. In other words, waveform patterns for each fault at any point

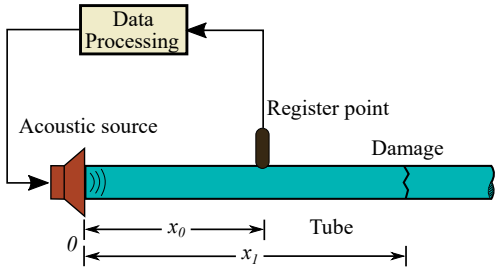

Fig. 1. Fault detection scheme for a pipeline with an acoustic source as a test signal

⋆ This work is supported by IT100519-DGAPA-UNAM and 280170conv2016-3 SENER-CONACyT.

of the conduit are determined. Two advantages of the proposed model is the generality in obtaining waveform patterns for diverse types of faults and the feasibility of its implementation with a single hardware device and pattern recognition algorithms.

The proposed analytical propagation model with faults can be applied to diverse boundary conditions and allows determining the fault patterns in time and frequency domains whenever a fault is present. In this presentation, a rigid body downstream and a short pulse pressure upstream are assumed to be the boundary conditions of the PDE. The damage scenarios are a blockage, a leak and a diameter reduction in the conduit. This contribution finishes by showing the waveform patterns from the transient responses of the pressure by simulation and the arriving time of the reflected wave by experimental data.

2. ACOUSTIC WAVE MODEL

This section derives the transfer matrix that describes the propagation of plane acoustic wave through a pipeline segment of length L with absorption because of viscosity. This model assumes the presence of faults at arbitrarily points of the pipeline.

2.1 Propagation model for a healthy section

Consider the linearized unidimensional model for acoustic waves in a pipeline (Blackstock, 2000):

$$-\frac{1}{\rho_0 c^2}\frac{\partial p(x,t)}{\partial t} = \frac{\partial u(x,t)}{\partial x} \tag{1}$$

$$\frac{\partial p(x,t)}{\partial x} + \rho_0 \frac{\partial u(x,t)}{\partial t} - \eta \frac{\partial^2 u(x,t)}{\partial x^2} = 0, \tag{2}$$

where $(x,t) \in [0,l] \times [0,+\infty)$ are the space [m] and time [s] coordinates. The variable $p(x,t)$ denotes the acoustic pressure variation, $u(x,t)$ is the particles velocity variation and ρ_0 is the medium density [kg/m^3] in equilibrium. Moreover, c is the speed of sound in the medium [m/s], and η is the fluid viscosity [kg/(m $\cdot$ s)].

To obtain the wave equation, the partial derivative with respect to x of (1) and the partial derivative with respect to t of (2) are taken respectively. Thus, one gets

$$\frac{\partial^2 u(x,t)}{\partial x^2} = -\frac{\eta}{\rho_0 c^2}\frac{\partial^3 u(x,t)}{\partial x^2 \partial t} + \frac{1}{c^2}\frac{\partial^2 u(x,t)}{\partial t^2}. \tag{3}$$

and by transforming (3) into the frequency domain with null initial conditions, one obtains

$$\frac{d^2 u(x,s)}{dx^2} = -\frac{\eta s}{\rho_0 c^2}\frac{d^2 u(x,s)}{dx^2} + \frac{s^2}{c^2}u(x,s) \tag{4}$$

which corresponds to the acoustic wave propagation equation

$$\frac{d^2 u(x,s)}{dx^2} = \gamma^2(s) u(x,s), \tag{5}$$

with $\gamma^2(s) = \frac{s^2}{c^2(1+\delta_v s)}$ as the propagation variable and $\delta_v = \eta/\rho_0 c^2$ as the friction factor caused by the viscosity.

By considering the boundary conditions at the ends of the line

$$\chi(0,s) = \begin{bmatrix} p(0,s) \\ u(0,s) \end{bmatrix}, \text{ and } \chi(l,s) = \begin{bmatrix} p(l,s) \\ u(l,s) \end{bmatrix} \tag{6}$$

the solution of (5) takes the form

$$u(x,s) = c_1(s)\sinh\gamma(s)x + c_2(s)\cosh\gamma(s)x. \tag{7}$$

and the functions $c_1(s)$ and $c_2(s)$ are calculated by (6).

On the other hand, by transforming (1) into the frequency domain the acoustic pressure can be written by

$$p(x,s) = -Z(s)\left(c_1(s)\cosh\gamma(s)x + c_2(s)\sinh\gamma(s)x\right), \tag{8}$$

where $Z(s) = \gamma(s)\rho_0 c^2/s$ is the acoustic impedance of the line. Thus, from (7) and (8) at upstream of the line ($x = 0$) the functions

$$c_1(s) = -\frac{1}{Z(s)}p(0,s) \quad \text{and} \quad c_2(s) = u(0,s), \tag{9}$$

are fixed. Therefore, the states of the fluid at the section extremes are related to

$$\chi(l,s) = M^l(s)\chi(0,s) \tag{10}$$

with the transfer matrix

$$M^l(s) = \begin{bmatrix} \cosh\gamma(s)l & -Z(s)\sinh\gamma(s)l \\ -\dfrac{\sinh\gamma(s)l}{Z(s)} & \cosh\gamma(s)l \end{bmatrix}. \tag{11}$$

This transfer matrix corresponds then to the model of a healthy pipeline of length l. The general model for a pipeline formed with additional components and healthy sections is developed in the next subsection.

2.2 Propagation model for sections interconnection

To develop the wave propagation model with faults, a pipeline of length L integrated by healthy sections connected to diverse components is considered. The two-port scheme given in Fig. 2 describes the pipeline block diagram with three intact sections connected by two components P_0 and P_1 and where the upstream boundary condition $\chi(0,s)$ is the acoustic source represented as the loudspeaker of Fig. 1, and $\chi(L,s)$ is the state at the external terminal associated with the downstream boundary condition.

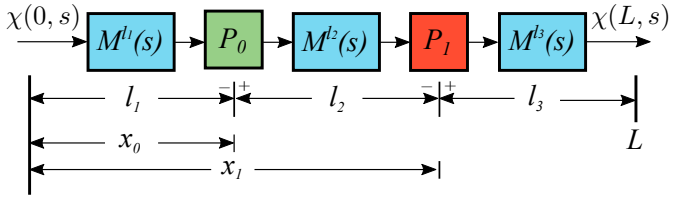

Fig. 2. Interconnected pipeline with a register point at x_0 and a damage defined by P_1 at point x_1

In this diagram the unit transfer matrix $P_0 = I$ is associated with a register point that represents the microphone, and P_1 is the two-port transfer matrix associated with any type of joint that characterizes a damage. Thus, the transfer matrix of the entire two-port system with a fault P_1 can be written by

$$\chi(L,s) = F^L(s)\chi(0,s), \tag{12}$$

with

$$F^L(s) = \begin{bmatrix} F^L_{11}(s) & F^L_{12}(s) \\ F^L_{21}(s) & F^L_{22}(s) \end{bmatrix} = M^{l_3}(s)P_1 M^{l_2}(s)P_0 M^{l_1}(s)$$

and the transfer matrices $M^{l_i}(s)$ are given by (11) and correspond to healthy pipeline sections of length l_i with $L = \sum_{i=1}^{3} l_i$.

Because the state at the register junction $\chi(x_0, s)$ satisfies both equations

$$\chi(x_0, s) = M^{l_1}(s)\chi(0, s) = \begin{bmatrix} M_{11}^{l_1}(s) & M_{12}^{l_1}(s) \\ M_{21}^{l_1}(s) & M_{22}^{l_1}(s) \end{bmatrix} \chi(0, s),$$

and

$$\chi(x_0, s) = \left(F^{\bar{l}_1}(s)\right)^{-1} \chi(L, s),$$

with $\bar{l_1} = L - l_1$ and

$$F^{\bar{l}_1}(s) = M^{l_3}(s)P_1M^{l_2}(s) = \begin{bmatrix} F_{11}^{\bar{l}_1}(s) & F_{12}^{\bar{l}_1}(s) \\ F_{21}^{\bar{l}_1}(s) & F_{22}^{\bar{l}_1}(s) \end{bmatrix},$$

the state at x_0 can be then expressed in terms of the upstream and downstream variables as

$$\chi(x_0, s) = \frac{1}{2}\left[M^{l_1}(s) \ \left(F^{\bar{l}_1}(s)\right)^{-1}\right] \begin{bmatrix} \chi(0, s) \\ \chi(L, s) \end{bmatrix}. \quad (13)$$

This transfer matrix by considering absorption loss is valid for any acoustic excitation source at the extremes of the line, plays an important role in obtaining the fault patterns in the line and has not been reported before.

2.3 Boundary conditions

To completely describe the fluid behavior in the pipeline with faults, the boundary conditions must be defined. Thus, the upstream pressure $p(0, s)$ is assumed to be the excitation acoustic source, and downstream a rigid body is assumed. Thus, the velocity at the downstream extreme $u(L, s) = 0$ when $L \longrightarrow \infty$. Under this condition, the upstream velocity $u(0, s)$ and the downstream pressure $p(L, s)$ can be calculated by (12). Thus, the boundary conditions are given in terms of acoustic source by

$$\chi(0, s) = \begin{bmatrix} 1 \\ -\frac{F_{21}^L(s)}{F_{22}^L(s)} \end{bmatrix} p(0, s), \ \chi(L, s) = \begin{bmatrix} \frac{\det F^L(s)}{F_{22}^L(s)} \\ 0 \end{bmatrix} p(0, s). \quad (14)$$

Therefore, from (13) and (14) one gets the transfer function between the acoustic source and the pressure at x_0 by

$$p(x_0, s) = G(s)p(0, s) \quad (15)$$

with

$$G(s) = \frac{1}{2}\left(M_{11}^{l_1}(s) + \frac{F_{11}^{\bar{l}_1}(s)\det F^L(s) - M_{12}^{l_1}(s)F_{21}^L(s)}{F_{22}^L(s)}\right). \quad (16)$$

By considering $P_1 = I$ as an interconnection point in the scheme after some simplifications, one obtains the transfer function of a healthy whole line

$$G_0(s) = \frac{\cosh\gamma(s)l_2}{\cosh\gamma(s)(l_1 + l_2)}. \quad (17)$$

By assuming that the distance from the acoustic source to the register point l_1 is smaller than the length L and by substituting the hyperbolic functions for exponential functions in (17), after some manipulations the transfer function is reduced to

$$G_0(s) = e^{-l_1\gamma(s)}. \quad (18)$$

Note that if the absorption effect is neglected, this transfer function is reduced to a pure delay. This means physically that the source signal $p(0, t)$ travels in the x direction and reaches the register point at the time $t_1 = l_1/c$. In addition, it continues traveling without return since the line is infinite.

An important property of the general transfer function (16) is the characterization of the signal $p(x_0, s)$ at the register point x_0 for diverse type of faults, if the corresponding matrix P_1 is used in (12). Three components with damage are managed in this work: a blockage, a diameter reduction and a leak. The next section describes the transfer functions associated with each fault.

2.4 Punctual fault transfer functions

According to Chaudhry (2013), any discontinuity in a conduit at position x_1 can be expressed as a two-port constant transfer matrix P_1 that relates the state of the fluid before and after the discontinuity condition.

Let x_1 be the position of the junction between two sections of a line with P_1 given according to the physical laws of the specific fault; the fluid states before and after the damage are then related by

$$\chi(x_1^+, s) = P_1\chi(x_1^-, s),$$

where $x_1^+ = x_1 + \varepsilon$, $x_1^- = x_1 - \varepsilon$ (with a small value $\varepsilon \to 0$). Table 1 describes parameters and matrices for the three considered faults taken from Munjal (1987) and Chaudhry (2013).

Table 1. Connection junction models

Scenario	Matrix	Description
Area reduction	$P_r = \begin{bmatrix} 1 & 0 \\ 0 & r_e \end{bmatrix}$	an area reduction in the conduit from s_1 to s_2 [m^2] where $r_e = s_1/s_2$
Leakage	$P_l = \begin{bmatrix} 1 & 0 \\ -\xi & 1 \end{bmatrix}$	ξ [m/(Pa·s)] depends on the speed ratio with regard to the nominal pressure
Blockage	$P_b = \begin{bmatrix} 1 & -B \\ 0 & 1 \end{bmatrix}$	B [(Pa·s)/m] depends on the size of the blockage, pressure loss and flow rate

3. FAULT PATTERNS

3.1 Fault pattern

By substituting the matrices of the fault connection junctions taken from Table 1 in (16), the transfer functions for each specific fault are generated. These transfer functions describe the relation between the wave source and the pressure $p(x_0, s)$ and are given in Table 2.

Since $l_3 \gg l_1 + l_2$, the respective transfer functions for the three faults given in Table 2 can be reduced to the general form

$$G_f(s) = e^{-l_1\gamma(s)}\frac{1 + \Gamma_f(s)e^{-2l_2\gamma(s)}}{1 + \Gamma_f(s)e^{-2(l_1+l_2)\gamma(s)}}, \quad (19)$$

where $\Gamma_f(s)$ is the reflection coefficient and characterizes the fault type. The specific coefficients for the three faults are given in Table 3.

In other words, for a given source waveform $p(0, s)$, the response $p(x_0, s)$ can be used to define the pattern for

Table 2. Transfer functions from $p(0,s)$ to $p(x_0,s)$

Reduction $G_r(s)$
$\dfrac{r_e \cosh\gamma(s)l_2 \cosh\gamma(s)l_3 + \sinh\gamma(s)l_2 \sinh\gamma(s)l_3}{r_e \cosh\gamma(s)(l_1+l_2)\cosh\gamma(s)l_3 + \sinh\gamma(s)(l_1+l_2)\sinh\gamma(s)l_3}$
Leakage $G_l(s)$
$\dfrac{\xi Z(s)\sinh\gamma(s)l_2 \cosh\gamma(s)l_3 + \cosh\gamma(s)(l_2+l_3)}{\xi Z(s)\sinh\gamma(s)(l_1+l_2)\cosh\gamma(s)l_3 + \cosh\gamma(s)(l_1+l_2+l_3)}$
Blockage $G_b(s)$
$\dfrac{(B/Z(s))\cosh\gamma(s)l_2 \sinh\gamma(s)l_3 + \cosh\gamma(s)(l_2+l_3)}{(B/Z(s))\cosh\gamma(s)(l_1+l_2)\sinh\gamma(s)l_3 + \cosh\gamma(s)(l_1+l_2+l_3)}$

Table 3. Reflection coefficients

Γ_r	$\Gamma_l(s)$	$\Gamma_b(s)$
$\dfrac{r_e-1}{r_e+1}$	$\dfrac{-\xi Z(s)}{\xi Z(s)+2}$	$\dfrac{B}{B+2Z(s)}$

each type of fault. For attaining the pattern of the signal at x_0, the feedback block diagram associated with (19) is considered. Fig. 3 shows the block representation with an input waveform $p(0,s)$ of short duration in comparison with L/c and the zero absorption factor through a simple derivation.

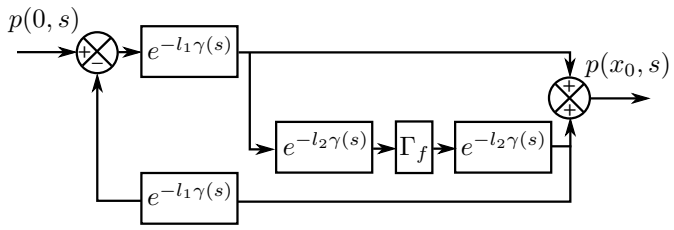

Fig. 3. Feedback block diagram for a fault in a pipeline

From the block diagram, one can generate the time response of the system following the paths of the feedback signals. In this way, for an intact pipeline $\Gamma_f(s) = 0$ and after $t_1 = l_1/c$, the input pressure signal $p(0,t)$ is visualized at the output, and this waveform does not return to the register point because the feedback is open.

On the other hand, in fault condition $0 < |\Gamma_f(s)| < 1$, a sequence of paths from $p(0,s)$ to $p(x_0,s)$ is performed. The waveform source first reaches the output at $t_1 = l_1/c$, and it also travels to the output by passing through the parallel path $e^{-2l_2\gamma(s)}\Gamma_f(s)$ and arriving at $t_2 = (l_1+2l_2)/c$. Furthermore, this second waveform returns to the output summation point after $2t_1$. This means that the waveform reaches the output at $t_3 = (3l_1+2l_2)/c$. Since the gain $\Gamma_f(s)$ is less than 1 for the faults considered, this attenuated waveform sequence is repeated each $t_r = 2(l_1+l_2)/c$ or equivalent to t_1+t_2.

Thus, following the waveform sequence described above, the dominant pattern of the output signal $p(x_0,t)$ can be schematized. Fig. 4 shows the impulse pressure response $p(x_0,t)$, assuming $\Gamma_f(s)$ a constant.

The pattern of Fig. 4 can be easily verified from the denominator of the transfer function of the feedback

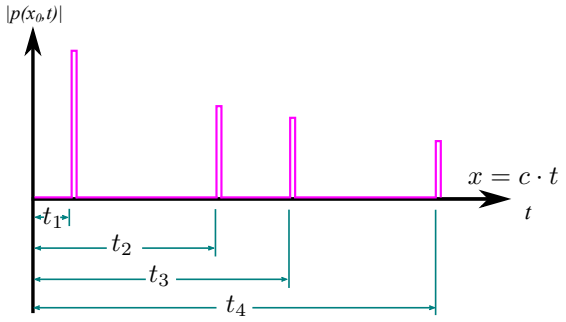

Fig. 4. Arriving time of the pattern of the waveform sequence at x_0 for an impulse

system (19) when the denominator is expanded through its binomial series. Since $|\Gamma_f(s)| < 1$, one obtains from the denominator after some manipulation

$$G_f(s) = e^{-l_1\gamma(s)} + \Gamma_f(s)e^{-(l_1+2l_2)\gamma(s)} - \Gamma_f(s)e^{-(3l_1+2l_2)\gamma(s)} - \Gamma_f^2(s)e^{-(3l_1+4l_2)\gamma(s)} + \ldots \quad (20)$$

One can see from this delay series that the first three terms are associated with the wave sequence generated from the feedback system and that each exponential term has the structure

$$g(s) = e^{c_1 s + c_2 s^2}. \quad (21)$$

Moreover, the repetition interval of the sequence is determined by the difference between the exponents of the fourth and second term from (20). As a consequence, this pattern has important properties from the fault detection point of view, and they are summarized in the following subsection.

3.2 Pattern features

From the waveform of Figure 4 and (20), one concludes the following features.

F1. The arrival time t_1 of the first returned signal is invariant with respect to the type of fault.
F2. The distance from the register point to any fault is associated with the time difference $t_2 - t_1$, and then the distance between the fault and the register point is given by $l_2 = \dfrac{t_2-t_1}{2}c$.
F3. The third waveform is generated by the reflection of the second wave at the time $t_3 = t_2 + 2t_1$.
F4. The feedback signals are always attenuated even in the absence of absorption.
F5. By taking into account the transfer functions $\Gamma_f(s)$, the following specific patterns are recognized.
  P1. For the leak case, the first reflected waveform has a phase opposite from the source since $\Gamma_l(s)$ is negative for low frequencies.
  P2. For the reduction case, Γ_r is a positive constant, and the first reflected wave has the same phase as the source.
  P3. For the blockage case, $\Gamma_b(s)$ is positive for low frequencies.
  P4. From the second term of (20), the specific fault parameter can be calculated for $\alpha_v = 0$ and $Z = \rho_0 c$. Thus, with $|\Gamma_f| = A_1$ the following fault parameters are obtained:

$$r_e = \frac{1+A_1}{1-A_1}; \xi = \frac{2}{\rho_0 c}\left(\frac{|A_1|}{1-|A_1|}\right); B = \frac{2\rho_0 c A_1}{1-A_1}. \tag{22}$$

In the case where $\alpha_v \neq 0$, these three relations are approximations.

Thus, from a practical point of view, one defines as the fault pattern only the first three waveforms given in Fig. 4 because the other waveforms are caused by the bounces between the fault and the acoustic source.

4. RESULTS

To exemplify the feasibility of obtaining a damaged conduit, two experiments were performed, one by simulation and the other with real data from a conduit of 4.85 $[m]$ of length.

4.1 Simulation results

To validate the pattern features by simulation, a pipeline with the parameters summarized in Table 4 is used.

Table 4. Parameter values for the simulation

$c =$	1 m/s	$\rho_0 =$	1 kg/m^3	$\alpha_v =$	0.0005 s^2/m
$x_0 =$	1 m	$x_1 =$	3 m	$a =$	0.1 s
$r_e =$	2	$\xi =$	0.8 m/Pa · s	$B =$	5 Pa · s/m

According to Lee et al. (2014), for providing satisfactory, accurate results for leak detection, the wave source at $x = 0$ must have a relatively high bandwidth. A pulse of short duration is then selected given by

$$p(0,s) = \frac{1}{s}\left(1 - e^{-as}\right), \tag{23}$$

where a specifies the pulse width in the test.

By considering only the first three terms of (20) and (23), the approximated output is

$$p(x_0,s) \cong (1-e^{-as})\frac{e^{-l_1\gamma(s)} + \Gamma_f(s)\left(g_1(s) - g_2(s)\right)}{s}, \tag{24}$$

where $g_1(s)$ and $g_2(s)$ have the structure given in (21). Finally, by approximating $\Gamma_f(s)$ by its first k-th terms of its binomial expansion and by substituting these terms $g_1(s)$ and $g_2(s)$ in (24), one can demonstrate that the numerator of (18) only has functions of the class

$$s^\beta \frac{g(s)}{s},$$

where $\beta \in \mathbb{N}$ and $g(s) = e^{c_1 s + c_2 s^2}$. Since the inverse transform of this function class is given by Campbell and Foster (1931),

$$\frac{1}{\sqrt{2\pi(2c_2)^\beta}} e^{\left(-\frac{t+c_1}{8c_2}\right)} D_{\beta-1}\left(-\frac{t+c_1}{\sqrt{2c_2}}\right)\mathcal{U}(t+c_1), \tag{25}$$

where $D_{\beta-1}(t)$ is the parabolic cylinder function of order $\beta - 1$ and $\mathcal{U}(t)$ is the Heaviside function, the pressure in the time domain $p(x_0,t)$ can be numerically approximated from (24) by using (25). In this work, the time evolution of the inverse transform of (24) has been implemented in Mathematica (Inc., 2018), and the number k in $\Gamma_f(s)$ is given such that the error $\Delta_p = |\, p(x_0,t)_k - p(x_0,t)_{k+1}\,| < 0.001$.

By considering the physical parameters of Table 4 and (24) and (25), the pressure waveforms for the three faults are simulated and shown in Fig. 5, 6 and 7.

From the three graphics one can verify that the pattern features of 3.2 satisfy the following.

- The waveforms reach the register point at $\hat{t}_1 = 1$ s, $\hat{t}_2 = 5$ s and $\hat{t}_3 = 7$ s for the three simulated cases and then $l_2 = 2$ m.
- For the reduction and blockage cases, the pressure at the register point is positive at $\hat{t}_2$. On the contrary, the pressure is negative for the leak case.
- The amplitudes of the second waveform are reduction: $A_1 = 0.281$, leak: $A_1 = 0.267$, and blockage: $A_1 = 0.655$.
- The waveform sequence is $\hat{t}_r = 6$ s.

Moreover, from the pressure of Fig. 6 one detects that the behavior of the pressure corresponds to a leak according to P1.

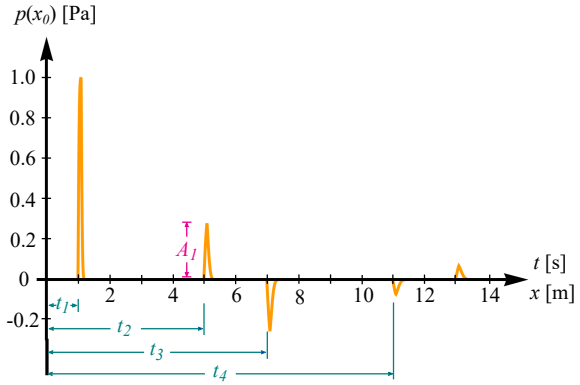

Fig. 5. Waveform of the pressure for a simulated reduction

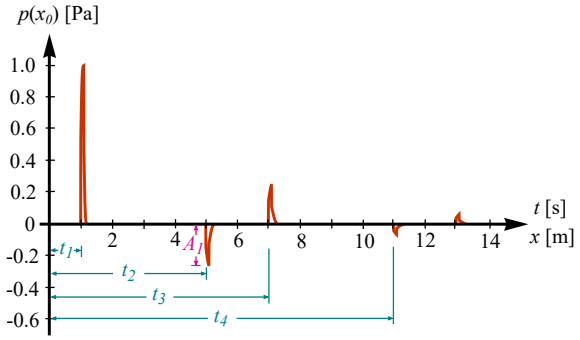

Fig. 6. Waveform of the pressure for a simulated leak

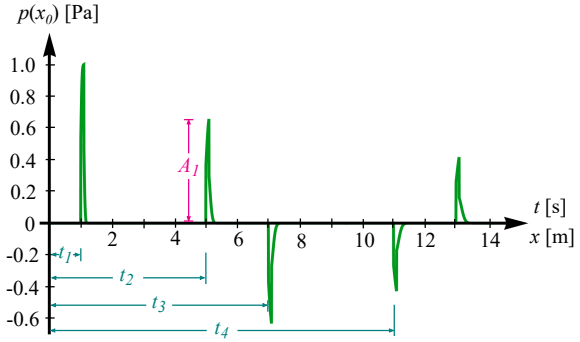

Fig. 7. Waveform of the pressure for a simulated blockage

From the pressure in Fig. 5 and 7, however, one can only identify that the damage was produced by a reduction or a blockage, but the damage cannot be isolated from the patterns.

With respect to the damage magnitudes, one can estimate the leak magnitude by using (22) and the amplitude $|A_1|$ of the second pressure waveform from Fig. 6. This means $\hat{\xi} = 0.729$ is close to the parameters of the damage used in the simulation ($\xi = 0.8$).

As a consequence, these simulation results validate the pattern features proposed in Section 3.

4.2 Experimental results

To validate the distance between the register point and any irregularity, a conduit of $PVC - U$ is instrumented. The acoustic source is fixed upstream from a conduit of length $4.85\,[m]$ joined with two standard couplings at $0.35\,[m]$ and $3.35\,[m]$ respectively. A muffler is located at the other extreme of the line and emulates a blockage. The microphone is used to register the patterns and is located at $0.35\,[m]$ from the source. The experiment consists of the generation of a wave with a piezoelectric speaker and the registration of the incident and reflected waves at the microphone. Fig. 8 shows the sampled signal during $0.04\,[s]$, and three waves can be identified.

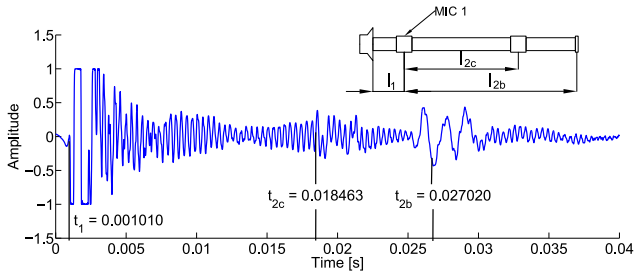

Fig. 8. Pulse response at the microphone

By considering the average arrived time for each wave marked in the graphic, one can estimate the positions of the microphone and the damages by considering a velocity $c = 343$ [m/s]. Thus, the estimated distance from the source to the microphone is given by $\hat{l}_1 = ct_1 = 0.34\,[m]$. For the distances from the microphone to the coupling and blockage one gets the estimations $\hat{l}_{2c} = \frac{c(t_{2c}-t_1)}{2} = 2.99.\,[m]$, and $\hat{l}_{2b} = \frac{c(t_{2b}-t_1)}{2} = 4.46\,[m]$ respectively. These estimations are coherent with the physical line and its irregularity with average errors less than $0.05\,[m]$.

5. CONCLUSIONS AND FUTURE WORK

This work developed an acoustic wave propagation model $G_f(s)$ in a pipeline with an absorption term caused by the viscosity of the gas for selecting the waveform patterns in fault conditions. An advantage of this model is that it allows generating patterns with discontinuous boundary conditions, instead of the models based on a Fourier description.

Based on the proposed model $G_f(s)$ with the absorption term, the characterization of the acoustic waves of three classes of faults was obtained: blockage, leakage and reduction of area, by assuming a pulse upstream from the pipeline as an acoustic source. Thus, the pattern signal given by the amplitude and arrival time of the wave at a register point for the three faults considered allowed the definition of fault features and the estimation of their magnitude. These patterns validated the empirical method given by Vidal and Silva (2014).

Although the results presented are not conclusive, they introduce the possibility of using pattern recognition algorithms to detect and locate damage in a gas pipeline with a simple maneuver, which can be implemented with a physical device based on acoustic emission.

REFERENCES

Ahadi, M. and Sarif-Bakhtiar, M. (2010). Leak detection in water-filled plastic pipes through the application of tuned wavelet transforms to acoustic emission signals. *Applied Acoustics*.

Blackstock, D. (2000). *Fundamentales of physical acoustics*. John Wiley and Sons.

Brunone, B. and Ferrante, M. (2001). Detecting leaks in pressurised pipes by means of transients. *J. Hydraul. Res.*, 39(5), 539–547.

Campbell, G.A. and Foster, R.M. (1931). *Fourier integrals for practical applications*. Technical publications (American Telephone and Telegraph Company).: Mathematical physics. Bell telephone laboratories.

Chaudhry, M.H. (2013). *Applied Hydraulic Transients*. SpringerLink: Bücher. Springer Science & Business Media, 3rd edition.

Datta, S. and Sarkar, S. (2016). A review on different pipeline fault detection methods. *Journal of Loss Prevention in the Process Industries*, 41, 97–106.

Inc., W.R. (2018). Mathematica, Version 11.3. Champaign, IL, 2018.

Lee, P., Vitkovsky, J., Lambert, M., Simpson, A., Liggett, J., Lee, P., Vítkovský, J., Simpson, M., and Liggett, J. (2005). Leak location using the pattern of the frequency response diagram in pipelines: a numerical study. *Journal of Sound and Vibration*, 284(3), 1051–1075.

Lee, P.J., Duan, H.F., Tuck, J., and Ghidaoui, M. (2014). Numerical and experimental study on the effect of signal bandwidth on pipe assessment using fluid transients. *Journal of Hydraulic Engineering*, 141(2), 04014074.

Liu, C., Li, Y., Fang, L., and Xu, M. (2017). Experimental study on a de-noising system for gas and oil pipelines based on an acoustic leak detection and location method. *International Journal of Pressure Vessels and Piping*, 151.

Meniconi, S., Brunone, B., Ferrante, M., and Massari, C. (2011). Transient tests for locating and sizing illegal branches in pipe systems. *Journal of Hydroinformatics, IWA*.

Munjal, M.L. (1987). *Acoustics of Ducts and Mufflers With Application to Exhaust and Ventilation System Design*. A Wiley-Interscience publication.

Verde, C. and Torres, L. (eds.) (2017). *Modeling and Monitoring of Pipelines and Networks*. Springer.

Vidal, J.L. and Silva, L.L. (2014). Acoustic reflectometry for blockages detection in pipeline. In *OTC Brasil*, 3382–3388. Offshore Technology Conference.